AIP | Journal of Applied Physics

Resonant absorption in semiconductor nanowires and nanowire arrays: Relating leaky waveguide modes to Bloch photonic crystal modes

Katherine T. Fountaine, William S. Whitney, and Harry A. Atwater

Citation: Journal of Applied Physics **116**, 153106 (2014); doi: 10.1063/1.4898758
View online: http://dx.doi.org/10.1063/1.4898758
View Table of Contents: http://scitation.aip.org/content/aip/journal/jap/116/15?ver=pdfcov
Published by the AIP Publishing

Resonant absorption in semiconductor nanowires and nanowire arrays: Relating leaky waveguide modes to Bloch photonic crystal modes

Katherine T. Fountaine,[1,2,a)] William S. Whitney,[2,3] and Harry A. Atwater[2,4]
[1]*Department of Chemistry and Chemical Engineering, California Institute of Technology, 1200 E. California Blvd., Pasadena, California 91125, USA*
[2]*Joint Center for Artificial Photosynthesis, California Institute of Technology, 1200 E. California Blvd., Pasadena, California 91125, USA*
[3]*Department of Physics, California Institute of Technology, 1200 E. California Blvd., Pasadena, California 91125, USA*
[4]*Department of Applied Physics and Materials Science, California Institute of Technology, 1200 E. California Blvd., Pasadena, California 91125, USA*

(Received 19 August 2014; accepted 9 October 2014; published online 21 October 2014)

We present a unified framework for resonant absorption in periodic arrays of high index semiconductor nanowires that combines a leaky waveguide theory perspective and that of photonic crystals supporting Bloch modes, as array density transitions from sparse to dense. Full dispersion relations are calculated for each mode at varying illumination angles using the eigenvalue equation for leaky waveguide modes of an infinite dielectric cylinder. The dispersion relations along with symmetry arguments explain the selectivity of mode excitation and spectral red-shifting of absorption for illumination parallel to the nanowire axis in comparison to perpendicular illumination. Analysis of photonic crystal band dispersion for varying array density illustrates that the modes responsible for resonant nanowire absorption emerge from the leaky waveguide modes. © *2014 AIP Publishing LLC*. [http://dx.doi.org/10.1063/1.4898758]

I. INTRODUCTION

Semiconductor nanowires have attracted much interest in the field of photovoltaics in recent years. This growing interest can be attributed to their numerous potential advantages over a traditional planar device, including (i) reduction of material usage, and thus cost, (ii) orthogonalization of the directions of light absorption and carrier collection, enabling higher quantum efficiencies for lower quality material,[1,2] (iii) relaxation of the lattice-matching requirement for tandem and multijunction devices via radial strain relaxation,[3,4] and (iv) light trapping phenomena that result in absorption enhancement.[5–8]

This study focuses on the light trapping properties of semiconductor nanowire arrays, which arise from their subwavelength features. Semiconductor nanowires and nanowire arrays can exhibit remarkable optical phenomena, such as reduced reflectance,[9–11] enhanced absorption,[12–15] and spectral selectivity,[16–18] which arise due to efficient coupling into discrete photonic modes. For individual nanowires, the photonic modes have been identified as leaky waveguide modes,[6,16] which are resonantly excited via illumination perpendicular to their axis. These modes are well-defined and well understood. For nanowire arrays, mode identification is less straight forward, due to the introduction of periodicity; absorption enhancements in nanowire arrays have been attributed to both leaky waveguide modes of individual nanowires[19–22] and photonic crystal Bloch modes.[12,23–26] Previous reports have examined a wide variety of array dimensions, nanowire geometries, and illumination angles, which also exhibit varying dominant mode resonances.

In this paper, we present a comprehensive explanation for resonant absorption into the leaky waveguide modes of semiconductor nanowires at varying illumination angles and the evolution of these modes into photonic crystal Bloch modes of nanowire arrays. The following analysis is performed on silicon nanowires ($r = 75$ nm and $L = 2\ \mu$m). We note that the lower absorption arising from the indirect bandgap of silicon facilitates distinction between modes closely spaced in frequency, but the conclusions are relevant for any high aspect ratio semiconductor nanowires, including direct bandgap materials (e.g., III-V compound semiconductor).

II. RESULTS AND DISCUSSION

A. Individual nanowires

A single semiconductor nanowire is a cylindrical dielectric waveguide with loss at frequencies above the band edge due to material absorption. From free space, the leaky modes of a cylindrical waveguide are accessible and result in resonant absorption due to field confinement in the high index wire. These leaky mode resonances are defined by Eq. (1), the eigenvalue equation for an infinitely long dielectric cylinder surrounded by air, derived from Maxwell's equations[27–29]

$$\pm\left(\frac{1}{k_{cyl}^2-k_{air}^2}\right)^2\left(\frac{k_z m}{k_0 a}\right)^2=\left(\frac{\varepsilon_{cyl}J_m'(k_{cyl}a)}{k_{cyl}J_m(k_{cyl}a)}-\frac{1}{k_{air}}\frac{H_m'(k_{air}a)}{H_m(k_{air}a)}\right)\times\left(\frac{1}{k_{cyl}}\frac{J_m'(k_{cyl}a)}{J_m(k_{cyl}a)}-\frac{1}{k_{air}}\frac{H_m'(k_{air}a)}{H_m(k_{air}a)}\right), \tag{1}$$

where m is the azimuthal mode order, a is the cylinder radius, ε_{cyl} is the complex permittivity of the cylinder, k_0 is the

a)Author to whom correspondence should be addressed. Electronic mail: kfountai@caltech.edu.

free space wavevector, k_{cyl} and k_{air} are the transverse components of the wavevector inside and outside of the cylinder, respectively, k_z is the wavevector along the cylinder axis, and J_m and H_m are the mth order Bessel and Hankel functions of the first kind, respectively. Through basic substitutions, this equation can be written in terms of k_0 and k_z, which describe the dispersion of each mode. Leaky waveguide modes are classified based on their azimuthal mode number, m, their radial mode number, n, which arises from the oscillatory behavior of the Bessel functions, and their polarization. Their polarization can be either TM (transverse magnetic, $H_z = 0$), TE (transverse electric, $E_z = 0$), HE (magnetoelectric, TM-like), or EH (electromagnetic, TE-like). The only modes that are strictly TE or TM for arbitrary wavevector are the 0th order azimuthal modes, TM_{0n} and TE_{0n}, and their solutions are found by setting the first and second term of the right hand side of Eq. (1) equal to zero, respectively. For $m > 0$, the HE and EH mode solutions can be found by selecting the $(+)$ and $(-)$ on the left hand side of the equation, respectively. The solutions to the eigenvalue equation ($k_0(k_z)$) are complex, where the real parts are indicative of the resonant wavelength and propagation constant and the imaginary part is indicative of the radiative loss of the mode, which for a lossless dielectric is a measure of the accessibility of a mode from free space and approaches zero (becoming inaccessible) as the mode transitions from leaky to guided ($k_z \rightarrow 0$ as $k_{air} \rightarrow 0$).[30] For a lossy dielectric, k_z is also a measure of the absorptive loss.

1. Illumination perpendicular to wire axis

The simplest case for analysis of this eigenvalue equation is illumination perpendicular to the nanowire axis. In this case, k_z is zero, the left hand side of the equation becomes zero, and all modes become either completely TM or TE, for any azimuthal order, m. As for the case of $m = 0$, described above, setting the 1st term (2nd term) of the right hand side of Eq. (1) equal to zero gives the TM (TE) modes. Table I summarizes the normalized eigenvalues, $k_0 r$, for a dielectric cylinder with a constant and real, index, $n_{cyl} = 4$. It is instructive to schematically analyze the mode eigenvalues for a real and constant index rather than a complex varying index of a real material such as silicon in order to make a fair comparison between two eigenmodes, specifically between their imaginary parts which become a convolution of radiative loss from the mode and absorption loss in the material when a complex index is used.

In general, the real part of the eigenvalue increases and the imaginary part of the eigenvalue decreases with increasing mode number, which indicates that higher order modes occur at higher frequencies (shorter wavelengths) and have less radiative loss, or in another light, are more difficult to couple to from free space, which implies smaller total absorption and smaller spectral width.[30]

To demonstrate the validity of the above analysis, we simulated absorption of a 75 nm radius silicon nanowire when illuminated perpendicular to its wire axis using full wave finite integration methods and a complex refractive index for Si. Figure 1 shows absorption efficiency, Q_{abs}, of the silicon nanowire (defined as its absorption cross section normalized to its physical cross section) as a function of wavelength for both TE- and TM-polarized incident light, with the spectral positions of leaky waveguide mode resonances within the 400–900 nm range indicated above along with profiles of the electric field intensity, $|E|^2$, for the nanowire cross section at the resonant wavelengths for the TM_{11}, TM_{21}, TM_{12}, TE_{01}, and TE_{11} modes. The inset of Fig. 1 illustrates the orientation for TE-polarization. In their displayed orientation, the light is first incident on the left side of the field profiles, causing them to be slightly distorted due to material absorption. The distortion is more prominent at shorter wavelengths where silicon absorbs more strongly. The peak spectral positions in Fig. 1 indicate that each of the modes predicted from Eq. (1) is excited; a subset of their field profiles is displayed at the top of Fig. 1 for visual verification of coupling into the predicted mode. The field profiles of these modes as determined from analytic theory can be

TABLE I. Leaky waveguide mode eigenvalues, $k_0 r$, for a dielectric cylinder with $n = 4$.

	n = 1		n = 2	
M	TE	TM	TE	TM
0	0.58–0.041i	0.20–0.089i	1.36–0.056i	0.99–0.068i
1	0.91–0.044i	0.58–0.041i	1.73–0.063i	1.36–0.056i
2	1.23–0.016i	0.93–0.013i	2.05–0.069i	1.72–0.036i

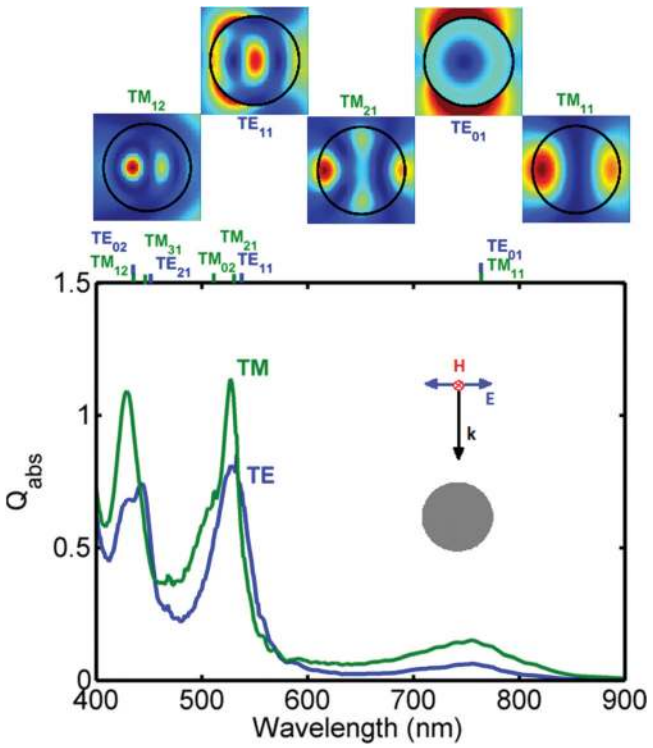

FIG. 1. Simulated absorption efficiency vs. wavelength for a silicon nanowire ($r = 75$ nm) illuminated perpendicular to its axis for both TE- (blue) and TM-polarized (green) light, with the inset showing the orientation for the TE-polarization; spectral positions of leaky mode resonances within the 400–900 nm wavelength range are indicated above accompanied by the observed electric field intensity profiles at the resonant wavelengths for the TM_{11}, TM_{21}, TM_{12}, TE_{01}, and TE_{11} modes.

found in Refs. 16 and 27–29. Peak spectral widths are smaller for higher order modes, as expected from the imaginary parts of the eigenvalues that decrease with increasing mode order. The overall absorption efficiency into each mode is influenced more strongly by the rapidly changing absorption coefficient of silicon, than by its eigenvalue.

2. Illumination parallel to the nanowire axis

For photovoltaic applications, vertically oriented nanowires are of primary interest, motivating analysis of illumination parallel to the nanowire axis. Figure 2 displays a plot of absorption efficiency vs. wavelength for a silicon nanowire ($r = 75$ nm and $L = 2\,\mu$m) illuminated parallel to its axis, with insets of the electric field intensity profiles for the nanowire cross section at the wavelengths of the two dominant absorption peaks at 445 nm and 800 nm. The closely spaced oscillations that becomes prominent when the absorption coefficients of silicon decreases dramatically beyond 550 nm are due to Fabry-Perot resonances, which are a product of the finite length of the wire. From the field profiles, it is clear that the peaks at the 445 nm and 800 nm can be attributed to the HE_{12} and HE_{11} leaky waveguide modes, respectively. The field profiles of these modes as determined from analytic theory can be found in Refs. 27–29. Note that these modes are related to the TM_{12} and TM_{11} modes from Subsection II A 1, but the introduction of a finite k_z results in the mode no longer being completely transverse magnetic.

For the case of an incoming wavevector aligned perfectly parallel to the nanowire axis ($k_z = k_0$), the transverse wavevector in air, k_{air}, becomes zero and the eigenvalue equation is ill-defined as the leaky modes transition into guided modes and are no longer accessible from free space. However, near the nanowire, the wave front of the free space plane wave is perturbed by the high index nanowire, introducing transverse components to the wavevector and enabling coupling into leaky waveguide modes. The overlap between the initial symmetry of the electric field of the incoming plane wave and that of the in-plane electric field of the HE_{1m} modes explains the preferential coupling into the HE_{11} and HE_{12} modes at normal incidence.[22,31] At other angles of incidence, this symmetry is broken and resonant absorption peaks for other leaky waveguide modes appear.

It is also interesting to note that the peak position of both the HE_{11} (800 nm) and the HE_{12} (445 nm) modes at parallel incidence are slightly red-shifted from those of the TM_{11} (765 nm) and TM_{12} (430 nm) modes at perpendicular incidence. This phenomena can be explained via the calculation of the full dispersion relation of the leaky waveguide modes, $k_0(k_z)$. Figure 3 displays the real parts of the dispersion relation for the TM-polarized modes, overlaid with the light line ($k_0 r = k_z r$) beyond which leaky modes transition to guided modes and are inaccessible from free space. The calculations were performed for a silicon nanowire with a radius of 75 nm, using the full complex refractive index of silicon. These dispersion curves illustrate the dependence of resonant wavelength, $k_0 = 2\pi/\lambda$, on angle of incidence, θ, which we can relate to k_z with a simple cosine relation: $k_z = k_0 \cos(\theta)$, so that $k_z = 0$ is illumination perpendicular to the wire axis and $k_z = k_0$ is illumination parallel to the wire axis. The TM-polarized modes with $m > 1$ are fairly flat, indicating minimal dependence of the spectral resonance on angle of illumination. The TM modes with $m \leq 1$ are fairly flat for small values of k_z, but become significantly perturbed as k_z approaches k_0. Specifically, the resonant position of the HE_{11} and HE_{12} modes shifts to lower frequencies or, equivalently, longer wavelengths. This case of k_z near k_0 is relevant for illumination parallel to the nanowire axis and explains the red-shift in peak positions of the HE_{11} and HE_{12} relative to those for illumination perpendicular to the nanowire axis.

B. Nanowire arrays

Vertically oriented nanowire arrays are the most relevant arrangement of nanowires for photovoltaic applications. Therefore, the next step in our analysis is to introduce periodicity. Fig. 4 displays simulated absorption vs. wavelength for a square-lattice array of silicon nanowires ($r = 75$ nm and $L = 2\,\mu$m) with 1000 nm spacing illuminated parallel to the nanowire axis, accompanied by the electric field intensity of the nanowire cross section at the two absorption peaks (440 nm and 775 nm). The absorption curve is qualitatively similar to the absorption efficiency curve of the individual

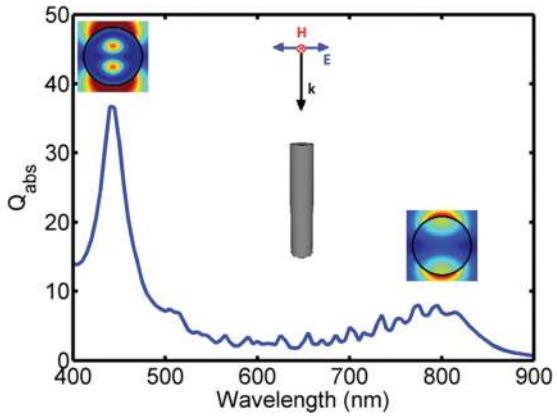

FIG. 2. Simulated absorption efficiency vs. wavelength for a silicon nanowire ($r = 75$ nm and $L = 2\,\mu$m) illuminated parallel to its axis (TEM polarization), with the inset showing the orientation and the electric field intensity profiles at the two main absorption peaks displayed above.

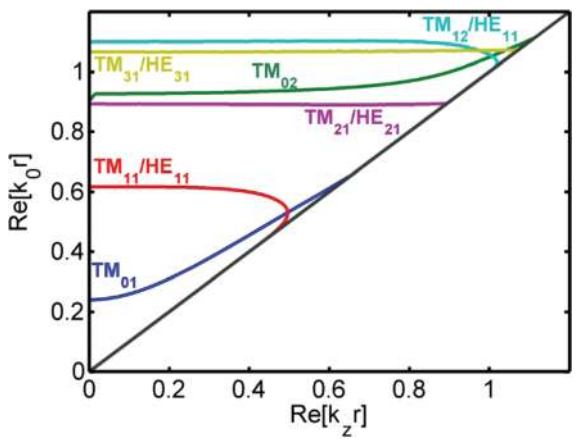

FIG. 3. Dispersion relation, $k_0 r(k_z r)$ for the TM-polarized eigenmodes of a silicon nanowire with radius of 75 nm.

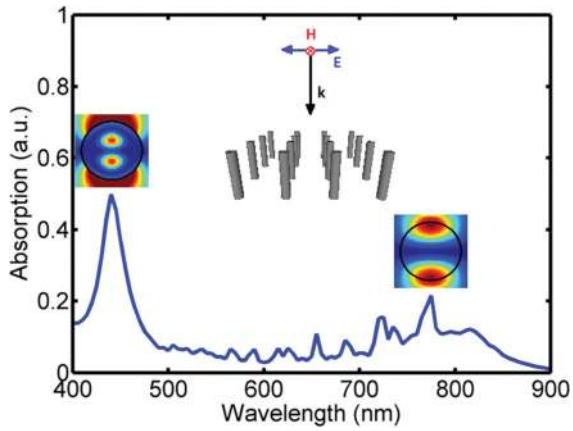

FIG. 4. Absorption vs. wavelength for a square-lattice array of silicon nanowires ($r = 75$ nm and $L = 2\ \mu$m) with 1000 nm spacing illuminated parallel to the nanowire axis, with inset for orientation and electric field intensity profiles at the absorption peaks displayed above.

nanowire (Fig. 3), with two dominant absorption peaks and closely spaced sharp oscillations beyond 550 nm. The electric field intensity profiles reveal that the absorption peaks correspond to resonant absorption into the HE_{11} and HE_{12} modes, as before, and the sharp oscillations are again attributed to Fabry-Perot resonances of the nanowire. These results indicate that leaky waveguide mode theory of individual wires is sufficient to describe sparse nanowire arrays.

Conceptually, the existence of leaky waveguide modes of single nanowires within an array is not obvious. A periodic array of nanowires is a 2D photonic crystal and thus any mode that propagates in the periodic plane is by definition a photonic crystal mode. To join these two concepts, we propose an extension of the analogy of the electronic crystal to the photonic crystal.[32] As isolated atoms move together to form a crystal, the isolated electronic energy levels of a single atom transition to electronic bands of a crystal. For atomic spacing, the isolated energy levels of a single atom are only slightly perturbed by the crystal lattice. Similarly, when inter-nanowire spacing is large, the isolated photonic modes of a nanowire are only slightly perturbed by the nanowire "lattice."[31,33,34]

To demonstrate this analogy, Fig. 5(a) displays the photonic crystal band diagrams for silicon nanowire arrays ($r = 75$ nm) with a lattice spacing of 150 nm (close-packed) and 250 nm. At larger spacings, the density of air mode bands becomes too high to distinguish them from the leaky waveguide modes that are localized around the nanowire. These band structures are overlaid with the frequency positions of the TM_{11}, TM_{21}, and TM_{12} leaky waveguide modes (black, flat lines), and the electric field intensity profiles for the photonic crystal bands nearest the leaky waveguide mode resonances are displayed to the side. Independent of nanowire spacing, the mode profiles of the bands nearest the leaky waveguide mode resonances correspond with the expected field profiles for the leaky waveguide modes, indicating that these are indeed the same photonic modes as for the single nanowire. Additionally, for the larger nanowire spacing, 250 nm, the photonic crystal bands corresponding to the leaky waveguide modes are nearly flat, indicating very weak dependence on the periodicity of the lattice. As the nanowire spacing decreases, these bands curve, indicate perturbation of the modes by the lattice. This perturbation is expressed in the mode profiles, which is more confined for close-packed nanowires.

A recent publication from Sturmberg *et al.* provides a more rigorous mathematical treatment of the connection between leaky waveguide modes and Bloch modes, which corroborates the above analysis.[34] They derive a modified version of the leaky waveguide eigenvalue equation for the first order ($m = 1$) modes that accounts for nearest neighbor

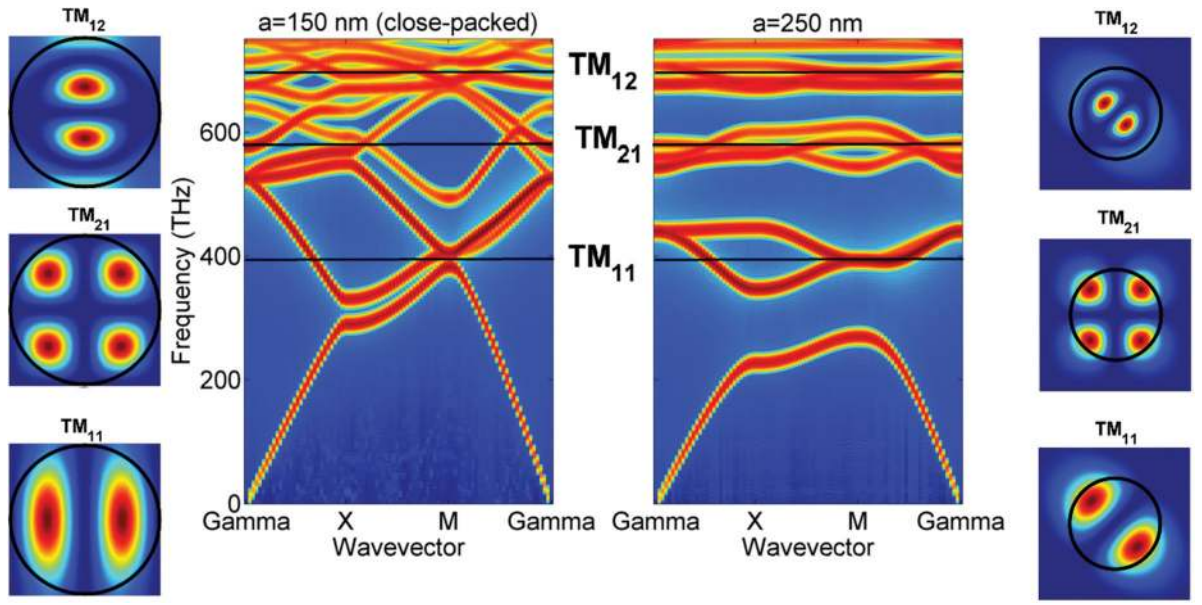

FIG. 5. Photonic crystal band diagrams for silicon nanowire arrays ($r = 75$ nm) for lattice spacings, $a = 150$ nm (close-packed) and $a = 250$ nm, overlaid with the positions of the TM_{11}, TM_{21}, and TM_{12} leaky waveguide modes (black, flat lines); electric field intensity profiles for the photonic crystal bands nearest the leaky waveguide mode resonances are displayed to the side.

interactions in infinitely periodic nanowire arrays. This eigenvalue equation is reproduced here, generalized for all mode orders, where S_0 is the first coefficient of the Rayleigh identity for an infinite lattice, representing the nearest neighbor interactions within the lattice

$$\left(\frac{\varepsilon_{cyl}}{k_{cyl}}\frac{J'_m(k_{cyl}a)}{J_m(k_{cyl}a)} - \frac{1}{k_{air}}\frac{H'_m(k_{air}a)+S_0J'_m(k_{air}a)}{H_m(k_{air}a)+S_0J_m(k_{air}a)}\right) \times \left(\frac{1}{k_{cyl}}\frac{J'_m(k_{cyl}a)}{J_m(k_{cyl}a)} - \frac{1}{k_{air}}\frac{H'_m(k_{air}a)+S_0J'_m(k_{air}a)}{H_m(k_{air}a)+S_0J_m(k_{air}a)}\right) = \pm\left(\frac{1}{k_{cyl}^2-k_{air}^2}\right)^2\left(\frac{k_z m}{k_0 a}\right)^2. \quad (2)$$

For sparse arrays of nanowires, coupling between nanowires is weak and, thus, S_0 is small; in the infinitely dilute limit, S_0 approaches zero and the modified eigenvalue equation for a nanowire array (Eq. (2)) reduces to the original waveguide eigenvalue equation for an individual nanowire (Eq. (1)). A positive value for S_0 indicates constructive interference of the fields of neighboring nanowires at their interfaces, and, conversely, a negative value indicates destructive interference. For $S_0 = 0.5$ (constructive interference), $k_z = 0$ and a constant, real index material ($n = 4$), the eigenvalue of the TM_{11} mode shifts from 0.58–0.041i (Table I) to 0.57–0.058i, revealing a red-shift in the resonant wavelength ($\sim$10 nm for a 75 nm radius nanowire) and an increase in the radiative loss of the mode, indicating a decrease in mode confinement. Larger, positive values of S_0 result in larger shifts in the same directions.

Conceptually, the red-shift and reduction in mode confinement emulates the effects of an increase in the refractive index of the surrounding medium; this apparent increase in refractive index of the surrounding medium is a localized effect at the nanowire interface due to the constructive interference of the fields. The opposite trend (blue-shifting and increased confinement) is observed for negative values of S_0, stemming from the destructive interference of fields and a localized apparent decrease in the refractive index of the medium. For a given structure, S_0 varies with k-vector, and therefore, the photonic crystal Bloch mode band can be blue- and red-shifted with respect to the leaky waveguide mode to which it corresponds (Fig. 5). As array density increases, the magnitude of S_0 increases due to stronger inter-nanowire coupling and, consequently, the photonic crystal Bloch mode band becomes more dispersive. This effect can be observed in Fig. 5 through the increased band-bending and confined field profiles of the close-packed nanowire arrays.

III. CONCLUSION

We have related the leaky waveguide modes of individual nanowires to absorbing modes of a 2D photonic crystal nanowire array, and demonstrated their role in absorption enhancements observed in nanowire arrays. The spectral positions of the leaky waveguide mode resonances were predicted using an eigenvalue equation derived from Maxwell's equations using analytic waveguide theory. The full dispersion relations derived from this equation explained the red-shifting of the HE_{11} and HE_{12} modes when illumination changed from perpendicular to parallel to the nanowire axis, and symmetry arguments explained the dominant coupling of a plane wave incident parallel to the nanowire axis into the HE_{11} and HE_{12} modes only. The leaky waveguide modes of individual nanowires are minimally perturbed by the addition of a lattice with large spacing, and thus, leaky waveguide mode theory can be used to describe the absorption behavior of sparse nanowire arrays.

IV. METHODS

All simulations were carried out in Lumerical FDTD (Finite Difference Time Domain), a full-field electromagnetic wave solver. The built-in Palik material data were used for silicon and all simulations were single wavelength to avoid inaccuracies from polynomial fits to the material data. For simulations with illumination perpendicular to the nanowire axis, 2D simulations were used and the nanowires were modeled as infinitely long cylinders. Perfectly matched layer (PML) boundary conditions were used on all sides to emulate infinite space. Simulations were carried out for wavelengths between 400 and 900 nm, every 1 nm. For illumination parallel to the nanowire axis, full-3D simulations were used. PML boundary conditions were used in all directions for the case of an isolated nanowire; for nanowire arrays, PML boundary conditions were used in the vertical z-direction and Bloch boundary conditions were used in the x- and y-directions to construct infinitely periodic square lattice arrays. Simulations were carried out for wavelengths between 400 and 900 nm, every 5 nm. Nanowire absorption was calculated using a transmission box around the nanowire. Absorption efficiencies for the single nanowire were calculated by normalizing absorption to the geometric cross section of the nanowire. Electric field intensity profiles for all simulations were recorded spatially using field and power monitors.

Photonic crystal calculations were performed using 2D simulations with Bloch boundary conditions to simulate infinite periodic arrays of nanowire structures in two dimensions. The band structure was calculated by determining the resonant frequencies present at each point in a parameter sweep of the photonic crystal wave vector, k. At each k-point, an individual, broadband simulation was performed for 0–750 THz. The mode excitation source was randomly positioned and randomly oriented dipoles with TM polarization were used. Time monitors collected the fields. Fast Fourier transform methods were used to compute the modal frequencies from the time domain field data. Mode profiles were calculated separately by exciting the system with a specific k-vector and frequency from a single TM-dipole source. The electric field profile across the unit cell was captured using a single, frequency-domain field monitor. A modified silicon material with an imaginary index of zero was used to mitigate rapid material absorption loss in the silicon and enable clearer Fourier transforms in the band structure calculation. The real index was unperturbed. For consistency, this material was also used for the mode profiles.

ACKNOWLEDGMENTS

This material is based upon work performed by the Joint Center for Artificial Photosynthesis, a DOE Energy Innovation Hub, supported through the Office of Science of the U.S. Department of Energy under Award No. DE-SC0004993. K.T.F. was supported by the National Science Foundation Graduate Research Fellowship under Grant No. DGE-1144469. W.S.W. was supported by the National Defense Science & Engineering Graduate Fellowship.

[1]B. Kayes, H. A. Atwater, and N. S. Lewis, "Comparison of the device physics principles of planar and radial p-n junction nanorod solar cells," J. Appl. Phys. **97**, 114302 (2005).
[2]M. D. Kelzenberg, S. W. Boettcher, J. A. Petykiewicz, D. B. Turner-Evans, M. C. Putnam, E. L. Warren, J. M. Spurgeon, R. M. Briggs, N. S. Lewis, and H. A. Atwater, "Enhance absorption and carrier collection in Si wire arrays for photovoltaic applications," Nat. Mater. **9**, 368 (2010).
[3]E. Ertekin, P. A. Greaney, D. C. Chrzan, and T. D. Sands, "Equilibrium limits of coherency in strained nanowire heterostructures," J. Appl. Phys. **97**, 114325 (2005).
[4]L. C. Chuang, M. Moewe, C. Chase, N. P. Kobayashi, C. Chang-Hasnain, and S. Crankshaw, "Critical diameter for III-V nanowires grown on lattice mismatched substrates," Appl. Phys. Lett. **90**, 043115 (2007).
[5]E. Garnett and P. Yang, "Light trapping in silicon nanowire solar cells," Nano Lett. **10**, 1082–1087 (2010).
[6]L. Cao, P. Fan, A. P. Vasudev, J. S. White, Z. Yu, W. Cai, J. A. Schuller, S. Fan, and M. L. Brongersma, "Semiconductor nanowire optical antenna solar absorbers," Nano Lett. **10**, 439–445 (2010).
[7]J. Kupec and B. Witzigmann, "Dispersion, wave propagation, and efficiency analysis of nanowire solar cells," Opt. Express **17**, 10399–10410 (2009).
[8]R. R. LaPierre, "Theoretical conversion efficiency of a two-junction III-V nanowire on Si solar cell," J. Appl. Phys. **110**, 014310 (2011).
[9]L. Hu and G. Chen, "Analysis of optical absorption in silicon nanowire arrays for photovoltaic applications," Nano Lett. **7**, 3249–3252 (2007).
[10]O. Muskens, J. G. Rivas, R. E. Algra, E. P. A. M. Bakkers, and A. Lagendijk, "Design of light scattering in nanowire materials for photovoltaic applications," Nano Lett. **8**, 2638–2642 (2008).
[11]P. Spinelli, M. A. Verschuuren, and A. Polman, "Broadband omnidirectional antireflection coating based on subwavelength surface Mie resonators," Nat. Commun. **3**, 692 (2012).
[12]C. Lin and M. L. Povinelli, "Optical absorption enhancement in silicon nanowire arrays with a large lattice constant for photovoltaic applications," Opt. Express **17**, 19371–19381 (2009).
[13]J. Li, H. Yu, S. M. Wong, X. Li, G. Zhang, P. G. Lo, and D. L. Kwong, "Design guidelines of periodic Si nanowire arrays for solar cell application," Appl. Phys. Lett. **95**, 243113 (2009).
[14]L. Wen, Z. Zhao, X. Li, Y. Shen, H. Guo, and Y. Wang, "Theoretical analysis and modeling of light trapping in high efficiency GaAs nanowire array solar cells," Appl. Phys. Lett. **99**, 143116 (2011).
[15]Z. Fan, R. Kapadia, P. W. Leu, X. Zhang, Y. L. Chueh, K. Takei, K. Yu, A. Jamshidi, A. A. Rathore, D. J. Ruebusch, M. Wu, and A. Javey, "Ordered arrays of dual-diameter nanopillars for maximized optical absorption," Nano Lett. **10**, 3823–3827 (2010).
[16]L. Cao, J. S. White, J. S. Park, J. A. Schuller, B. M. Clemens, and M. L. Brongersma, "Engineering light absorption in semiconductor nanowire devices," Nat. Mater. **8**, 643–647 (2009).
[17]S. K. Kim, R. W. Day, J. F. Cahoon, T. J. Kempa, K. D. Song, H. G. Park, and C. M. Lieber, "Tuning light absorption in core/shell silicon nanowire photovoltaic devices through morphological design," Nano Lett. **12**, 4971–4976 (2012).
[18]K. Seo, M. Wober, P. Steinvurzel, E. Schonbrun, Y. Dan, T. Ellenbogen, and K. B. Crozier, "Multicolored vertical silicon nanowires," Nano Lett. **11**, 1851–1856 (2011).
[19]S. Hu, C. Chi, K. T. Fountaine, M. Yao, H. A. Atwater, P. D. Dapkus, N. S. Lewis, and C. Zhou, "Optical, electrical, and solar energy–conversion properties of gallium arsenide nanowire-array photoanodes," Energy Environ. Sci. **6**, 1879–1890 (2013).
[20]K. T. Fountaine, C. G. Kendall, and H. A. Atwater, "Near-unity broadband absorption designs for semiconducting nanowire arrays via localized radial mode absorption," Opt. Express **22**(S3), A930–A940 (2014).
[21]G. Grzela, R. Paniagua-Dominguez, T. Barten, D. van Dam, J. A. Sanchez-Gil, and J. G. Rivas, "Nanowire antenna absorption probed with time-reversed Fourier microscopy," Nano Lett. **14**, 3227–3234 (2014).
[22]B. Wang and P. W. Leu, "Tunable and selective resonant absorption in vertical nanowires," Opt. Lett. **37**(18), 3756–3758 (2012).
[23]A. Deinega and S. John, "Solar power conversion efficiency in modulated silicon nanowire photonic crystals," J. Appl. Phys. **112**, 074327 (2012).
[24]L. Hong, Rusli, X. Wang, H. Zheng, H. Wang, and H. Y. Yu, "Design guidelines for slanting silicon nanowire arrays for solar cell application," J. Appl. Phys. **114**, 084303 (2013).
[25]A. Chutinan and S. John, "Light trapping and absorption optimization in certain thin-film photonic crystal architectures," Phys. Rev. A **78**, 023825 (2008).
[26]B. C. P. Sturmberg, K. B. Dossou, L. C. Botten, A. A. Asatryan, C. G. Poulton, C. Martijn de Sterk, and R. C. McPhedran, "Modal analysis of enhanced absorption in silicon nanowire arrays," Opt. Express **19**, A1067–1081 (2011).
[27]A. W. Snyder and J. D. Love, *Optical Waveguide Theory* (Springer, 1983).
[28]L. Cao, *Optical Resonances of Semiconductor Nanowires* (Stanford University, 2010).
[29]G. Grzela, *Directional Light Emission and Absorption by Semiconductor Nanowires* (Eindhoven University of Technology, 2013).
[30]Y. Yu and L. Cao, "Coupled leaky mode theory for light absorption in 2D, 1D, and 0D semiconductor nanostructures," Opt. Express **20**, 13847–13856 (2012).
[31]N. Anttu and H. Q. Xu, "Efficient light management in vertical nanowire arrays for photovoltaics," Opt. Express **21**, A558–A575 (2013).
[32]J. D. Joannopoulos, S. G. Johnson, J. N. Winn, and R. D. Meade, *Photonic Crystals: Molding the Flow of Light*, 2nd ed. (Princeton University Press, 2008).
[33]C. Vandenbem and J. P. Vigneron, "Mie resonances of dielectric spheres in face-centered cubic photonic crystals," J. Opt. Soc. Am. A **22**(6), 1042–1047 (2005).
[34]B. C. P. Sturmberg, K. B. Dossou, L. C. Botten, A. A. Asatryan, C. G. Poulton, R. C. McPhedran, and C. Martijn de Sterke, "Optimizing photovoltaic charge generation of nanowire arrays: A simple semi-analytic approach," ACS Photonics **1**, 683–689 (2014).